Experimental Study of Concrete Normal Mode Cohesive behavior at the Centimeter Scale

Joffrey Lhonneur, Moulay Saïd El Youssoufi, Frédéric Jamin, Yann Monerie, Celine Pelissou

Available online at www.sciencedirect.com

ScienceDirect

Procedia Structural Integrity 42 (2022) 513–521

Structural Integrity Procedia

www.elsevier.com/locate/procedia

23 European Conference on Fracture - ECF23

Experimental Study of Concrete Normal Mode Cohesive behavior at the Centimeter Scale

J. Lhonneur[a,c,*], M.-S. El Youssoufi[b,c], F. Jamin[b,c], Y. Monerie[b,c] and C. Pélissou[a,c]

[a]*IRSN, B.P.3, 13115 Saint-Paul-Lez-Durance Cedex, France*
[b]*LMGC, Université de Montpellier, CNRS, France*
[c]*MIST Lab, IRSN, CNRS, Université de Montpellier, France*

Abstract

Concrete rupture is mainly influenced by the mechanisms occurring at the scale of the Interfacial Transition Zone (ITZ) between cement matrix and aggregates. However, experimental quantitative assessment of concrete cohesive behavior at that scale (centimeter scale) remains an open issue among the scientific community.
In this paper, we present a three-point bending test allowing for a measure of the mechanical response of centimeter concrete samples. CEM I Portland cement paste sample, as well as composites cement-silica and cement-steel samples are tested.
Weibull parameters for estimating the probability of crack initiation in concrete at the centimeter scale are computed based on the experimental results.
A device for recording crack position on the surface of a sample is introduced. Its use in future studies might bring information on the crack dynamic propagation in concrete at the centimeter scale.

Keywords: Weibull; Concrete; Interface; Cohesive behavior; Rupture; Coupled Criterion.

1. Introduction

The Interfacial Transition Zone (ITZ) between cement matrix and aggregates plays a significant role on concrete rupture mecanisms (Simonova et al. (2017); Samal et al. (2019)). However, the characterization of ITZ mechanical behavior at the “interfacial/centimeter scale” has been the subject of few studies (Gu et al. (2013), Mielniczuk et al. (2016), Jebli et al. (2018)).

10.1016/j.prostr.2022.12.065

* Corresponding author. *E-mail address:* joffrey.lhonneur@irsn.fr

Nomenclature

F	Ultimate strength
p_f	Probability of failure of a flaw
P_s	Sample survival probability
P_f	Sample failure probability
φ	Characteristic Weibull function
m	Weibull shape parameter
F_{eq}	Weibull scale parameter
v^{mean}	Average crack speed
U_0	Imposed DC voltage in the crack speed monitoring device
R	Fixed resistor used for measuring crack speed
U_m	Measured voltage across the fixed resistor R
I	Electric current in the circuit used for crack speed measure
R_{eq}	Equivalent resistance of the conductive paint pattern
U_0	Imposed DC voltage in the crack speed monitoring device
n	Number of paint stripes not cut by the crack
R_p	Electric resistance of one paint stripe
h_0	Total height of the paint stripes set
h	Height of the crack

To our knowledge, only direct tensile tests have been performed at the centimeter scale on concrete samples for studying normal mode failure. It is well known that such tests are difficult to carry out on concrete samples and require the consideration of specific features. For example, Gu et al. (2013) carried out pull-off tests by using a specific device ("Limpet Pull-Off") on cylindrical CEM I 42.5 R Portland cement parts ($\emptyset\ 50\ mm \times 60\ mm$) poured on a marble plate (Fig. 1.a). Mielniczuk et al. (2016) considered a CEM II/B-LL 32.5 N cement paste confined between two pierced quartz pearls. They performed direct tensile tests by fixing the samples to the tensile test device with pins placed in the pearls holes (Fig. 1.b). Jebli et al. (2018) glued steel fixations on two parallelepiped limestone parts linked by a CEM II/B-LL 32.5 N cement paste (Fig. 1.c).

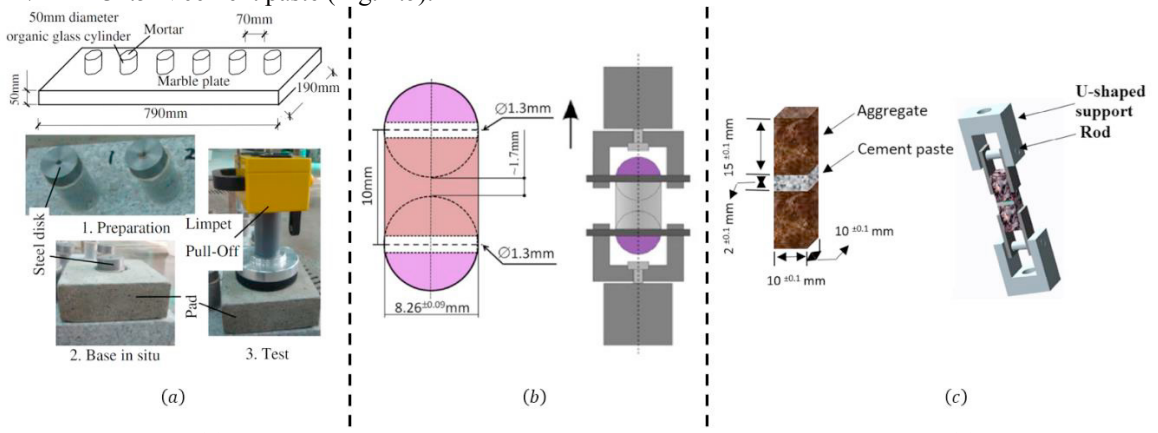

Fig. 1. Direct tensile tests. (a) Pull-off tests on cylindrical cement parts poured on a marble plate (Gu et al. 2013); (b) Direct tensile test on a cement-quartz composite (Mielniczuk et al. 2016); (c) Direct tensile test on a cement-limestone composite (Jebli et al. 2018).

The direct tensile test proposed by Jebli et al. (2018) (Fig. 1.c) has been analyzed by Malachanne et al. (2018) for estimating normal mode cohesive parameters of the cement-limestone interface which permit reproducing by numerical simulations the mechanical response of the parallelepiped cement-limestone composite under direct tensile tests. A similar study has been proposed by Salah et al. (2019) for estimating tangential mode cohesive parameters of

a cement-limestone interface. However, the experimental results in which these last two studies are based do not contain any information on the crack propagation mechanisms in samples. In fact, only a criterion for crack onset (in this case a critical stress) can be extracted from the direct tensile tests described hereabove.

Indeed, in the direct tensile test, it is possible to compute the cohesive energy (energy dissipated by unit crack surface) only in the case for which residual kinetic energy in the sample is neglectable (the cohesive energy being then the overall mechanical energy brought to the sample divided by the crack surface). When brittle samples are tested (e.g., the centimeter concrete samples) this condition is not fulfilled.

In this study, we present an indirect tensile test (a three-point bending test) for measuring the mechanical response of a CEM I Portland cement paste and of two types of composite samples at the centimeter scale: cement-steel and cement-silica composites.

The three-point bending test allows for the study of dynamic crack behavior as the crack would propagate with a finite speed depending on materials properties (including its cohesive ones) from an identified locus (in contrast to the tensile test in which the theoretical crack propagation speed is expected to be infinite whatever the materials properties).

Samples geometries considered in the present study induce the appearance of a single crack during the three-point bending tests. An experimental device is proposed for monitoring crack tip position at samples surface. It is expected that the information brought by the recording of both mechanical responses and cracks position in time would suffice for estimating both the normal mode critical cohesive stress and the normal mode cohesive energy used for example in cohesive zone models (Martin et al. 2016) as well as in Leguillon's Coupled Criterion (Leguillon 2002).

A Weibull statistical analysis of the ultimate strength recorded for each type of sample is presented. The obtained results might be used in future studies for estimating stochastic normal mode cohesive parameters of both a cement paste and an interface between a cement paste and an aggregate at the centimeter scale.

2. Materials and method

2.1. Samples preparation

The cement paste used was a Portland CEM I 52.5R CE CP2 NF from the Beaucaire quarry. A Water/Cement ratio of 0.5 has been considered. Parallelepiped steel parts ($10 \times 10 \times 15\ mm^3$) were cut from E24 S235 steel bars of desired cross section ($10 \times 10\ mm^2$) with a band saw. Silica parts of the same dimension ($10 \times 10 \times 15\ mm^3$) were obtained by cutting silica blocks. A coarse cut is first realized by using a diamond saw typically used for lithographic sample preparation. A second cut is then carried out in a fully automatized cutting device for obtaining the desired dimension with a precision of about $\pm\ 0.5\ mm$.

Three types of parallelepiped samples have been realized:

- notched cement pastes;
- cement-silica composites;
- cement-steel composites.

Geometry details are provided on Fig. 2. The notch introduced in the cement paste samples constrains the crack localization in the samples enhancing the test reproducibility. Composites samples do not have a notch as it is expected that cracks would "naturally" been localized at the cement-aggregate interface.

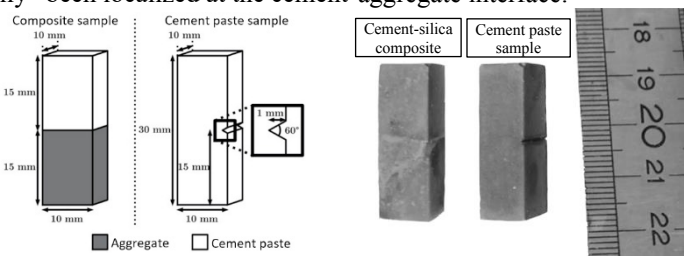

(a) (b)

Fig. 2. (a) Samples description; (b) Pictures of actual samples.

Silicone molds have been used to control the cement paste shape. For the composite samples, the steel or silica part is first introduced vertically in the mold cavity and the cement paste is then poured over till the complete filling of the cavity. Geometric details as well as images of actual samples are given in Fig. 2.

Immediately after cement pouring, the silicone molds are placed in a humid atmosphere (≥ 90 % of relative humidity) for 24 hours. Samples are then extracted from the molds cavities and fully immersed in a lime saturated distilled water at room temperature for preventing leaching. They are kept in the conservation bath until being tested.

2.2. The three-point bending test

A three-point bending test device has been manufactured for carrying out experimental investigations at the centimeter scale. The two supports on which samples are positioned (see Fig. 3) are fixed in a movable part which can slide along a rail for choosing the relative positioning of the three loading points. In the present study, the movable part position has been calibrated for realizing centered three-point bending tests (a clamping screw maintains its position during the tests).

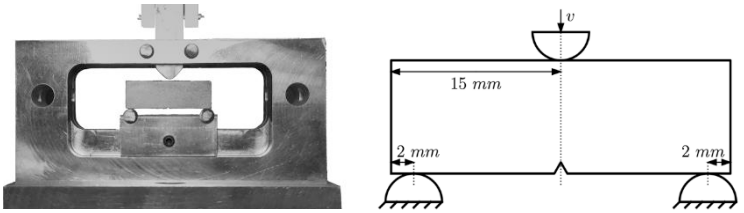

Fig. 3. (a) Three-point bending test device; (b) Sample positions during the tests.

Samples are positioned as explained in Fig. 3 and a quasi-static loading (loading speed $v = 10\ \mu m.s^{-1}$) is imposed up to samples rupture. A $500\ N$ force sensor has been used.

3. Results

3.1. Mechanical responses

All specimens have been tested after 28 days of hydration immediately after having been withdrawn from the conservation bath for limiting drying shrinkage effects. Mechanical responses are displayed in Fig. 4. A fragile behavior is observed with an average ultimate strength of $131\ N$ for both cement paste and cement-steel composite samples and of $158\ N$ for the cement-silica composite sample. A single crack appears at the samples half-length (i.e., above the notch in the cement paste samples and between cement and aggregate parts in composite samples) and propagates quasi-instantaneously.

Ultimate strength values measured in cement paste samples show a relatively good reproducibility of the three-point bending test. More scattered results have been obtained with composite samples. They suggest a stochastic interfacial cohesive behavior at the centimeter scale. Statistics of ultimate strength are gathered in Table 1.

Table 1. Ultimate strength statistics.

Sample type	Samples nb.	1^{st} quartile (N)	Median (N)	3^{rd} quartile (N)	Mean (N)	Standard deviation (N)
Cement paste	24	126	131	134	131	7.8
Cement-steel	30	112	130	139	131	22.9
Cement-silica	29	144	160	171	158	23.8

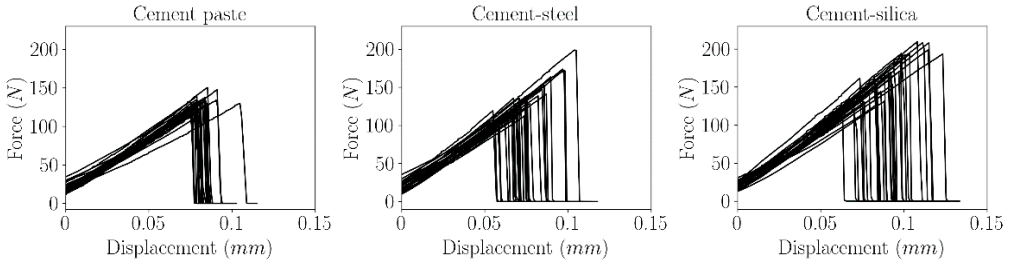

Fig. 4. Mechanical responses.

The Weibull law is often used for representing the stochastic nature of the ultimate strength measured on fragile materials. In the Weibull statistical theory of strength, the stochastic nature of the failure behavior is explained by a weakest link effect. Let us consider that n flaws are localized in the solicited sample volume, each having the same probability $p_f(F)$ of failure for an imposed force less than F. The sample survival probability $P_s(F)$ for an imposed force F is equal to the probability that each of the n flaws would not fail for a force less than F:

$$P_s(F) = \left(1 - p_f(F)\right)^n \tag{1}$$

As function P_s is positive and less than 1, it may be expressed as follows:

$$P_s(F) = exp\left(-n\varphi(F)\right) \tag{2}$$

where φ is a positive, not decreasing function which tends to zero when F tends towards zero. Weibull proposed to use the following form for φ:

$$\varphi(F) = \left(\frac{F}{F_c}\right)^m \tag{3}$$

where m is a shape parameter and F_c is a scale parameter.

The probability $P_f(F)$ of failure of a sample for a loading force less than F is then expressed as:

$$P_f(F) = 1 - P_s(F) = 1 - exp\left(-n\left(\frac{F}{F_c}\right)^m\right) = 1 - exp\left(-\left(\frac{F}{F_{eq}}\right)^m\right) \tag{4}$$

with F_{eq} an equivalent scale parameter depending on the solicited sample volume.

Equation (4) may be rewritten as follow:

$$ln\left(-ln\left(1 - P_f(F)\right)\right) = m\,ln(F) - ln\left(F_{eq}\right) \tag{5}$$

Values of Weibull parameters m and F_{eq} obtained for each type of samples by a linear regression are displayed in **Error! Not a valid bookmark self-reference.**.

Table 2. Weibull parameters for the three types of samples.

Sample type	m	F_{eq} (N)	R^2
Cement paste	20.1	2.35×10^{-43}	0.978
Cement-steel	7.13	5.57×10^{-16}	0.957
Cement-silica	6.72	8.91×10^{-16}	0.989

The higher values of F_{eq} obtained for the composite samples underline the fact that the cement-aggregate interface cohesive behaviors are more scattered than the cement paste one. Linear regression is relatively accurate for the cement-silica composite samples and is less accurate for the two other types of samples.

4. Development of a crack tip monitoring device

4.1. The device principle

A set of parallel conductive black paint stripes (stripes thickness: $0.5\ mm$, inter-stripe space: $1\ mm$) is positioned on samples between two pieces of conductive tape (see Fig. 5). Paint stripes have been made using a sticker serving as a stencil (stickers have been manufactured by a sticker printer).

The conductive tapes are then plugged in a circuit powered by a DC voltage $U_0 = 5\ V$. Instantaneous electrical current passing through the circuit is measured by using a voltmeter connected across a fixed resistor. Its value is directly linked to the number n of paint stripes through which the electrical current flows. As the crack propagates on the specimen surface, it progressively cuts the paint stripes decreasing n.

The crack speed is negligible in comparison to the electromagnetic field wave speed across the circuit. A quasi-stationary electric field is thus considered in the circuit at any time: in particular, the current value $I(t)$ verifies both following equations:

$$\begin{cases} U_0 - U_m(t) = R_{eq} \times I(t) & (6) \\ U_m(t) = R \times I(t) & (7) \end{cases}$$

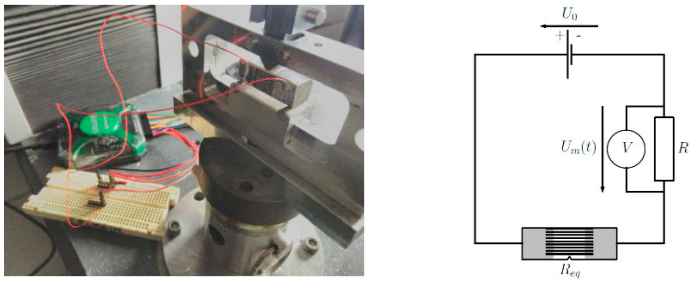

(a) (b)

Fig. 5. (a) Picture of a cement paste sample equipped with the conductive device for crack speed recording; (b) Scheme of the electrical assembly used for crack speed recording.

Substituting equation 67 into equation **Error! Reference source not found.** allows to link the equivalent resistance of the set of conductive paint R_{eq} to the imposed DC voltage U_0 as well as to the measured one $U_m(t)$ across the fixed resistor R:

$$R_{eq}(t) = R\,\frac{U_0 - U_m(t)}{U_m(t)} \quad (8)$$

Making the hypothesis that each stripe paint has relatively the same resistance R_p, the equivalent resistance R_{eq} verifies:

$$R_{eq}(t) = \frac{R_p}{n(t)} \quad (9)$$

Therefore, using equations (8) and (9), the number $n(t)$ of remaining paint stripes which have not been cut by the crack may be estimated by the following formula.

$$n(t) = \frac{Rp}{R}\left(\frac{U_m(t)}{U_0 - U_m(t)}\right) \tag{10}$$

As stripes are equally spaced along the crack path, there exists an affine relation between the number of remaining stripes $n(t)$ and the height of the crack $h(t)$. Therefore, using equation (10) and introducing the reduced voltage $u_r(t) = U_m(t)/\big(U_0 - U_m(t)\big)$ as well as the final height reach by the crack h_0, the crack height verifies:

$$h(t) = h_0\left(1 - \frac{u_r(t)}{u_r(0)}\right) \tag{11}$$

Signal h is by construction a staircase signal underestimating the actual value of the crack height. It is thus convenient to consider the convex envelop of the signal h which is piecewise linear and permits an estimation of the average crack speed when the crack is traveling between two adjacent stripes (see Fig. 6).

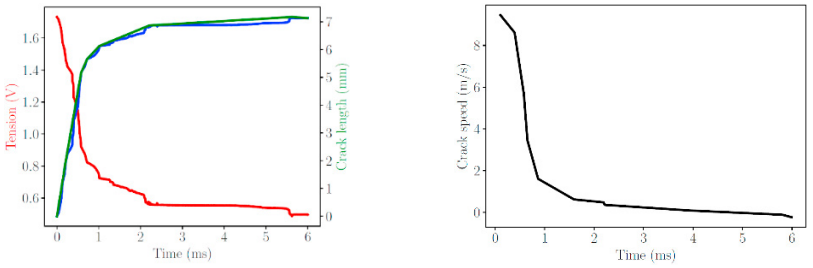

(a) (b)

Fig. 6. (a) An example of a recorded voltage (red) along with the corresponding crack length estimation (blue) and the convex envelop of the crack length estimation signal (green); (b) Crack speed estimation as a function of time.

4.2. First use of the device at a mesoscopic scale

The electronic device has been used on a notched parallelepiped concrete sample ($840 \times 100 \times 100\ mm^3$, notch depth: $50\ mm$, CEM I 52.5 R, S/C $= 3.0$ and W/C $= 0.5$) tested under a three-point bending test. In this test, a unique crack appears and slowly propagates vertically above the notch (see Fig. 7.a).

To assess the device measurements, a camera has been simultaneously used for recording the propagation of the crack tip through the paint stripes. The video has been analyzed using an image processing routine based on morphological mathematics. Fig. 7.b**Error! Reference source not found.** shows the comparison between the crack tip position computed by both devices.

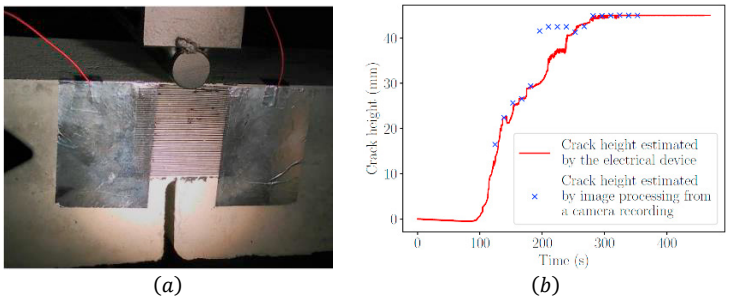

(a) (b)

Fig. 7. (a) Use of the electronic device for crack monitoring on a mesoscopic concrete sample. (b) Crack tip position in time: comparison between the electronic device measurements and a camera acquisition.

Although a difference is observed around 200 s, it has been estimated that this error would be due to the image processing algorithm whose precision is not optimal. In conclusion, it has been stated that the electrical device could be used for estimating with a relatively good accuracy the position of a crack tip in time evolving at the surface of a concrete sample.

4.3. Issues concerning crack speed recording at the centimeter scale: drying shrinkage effects

The use of the electronic device requires the sample surface on which it must be positioned to be dry enough. First attempts to dry surface of the centimeter samples conducted to a drastically change in samples behavior: samples were dried at free air during 24 hours before positioning the electrical device on them.

Unfortunately, drying shrinkage effects have led to the failure of all composite samples as well as a pre-initiation of the unique crack developing above the notch of all the cement paste samples inducing a loss of strength as well as the impossibility to use adequately the electrical device (which should not be positioned over a pre-cracked zone).

5. Conclusion

Three-point bending tests have been performed on parallelepiped concrete samples at the centimeter scale. It has been shown that ultimate strengths follow a Weibull statistical distribution with a relatively good accuracy. The Weibull parameters identified in this study give information on the stochastic nature of the normal mode onset criterion in a cement paste as well as at the interface between cement and aggregates in concrete.

The speed of the crack propagating at the samples surface could be obtained by using high frequency acquisition devices as a high-speed camera or an electrical device. Such a device has been proposed in the present paper and its use on concrete specimens for evaluating crack tip position in time at a sample surface has been validated.

However, it requires the sample surface to be dried. Unfortunately, this last requirement seems to be difficult to fulfill on centimeter samples highly sensible to drying shrinkage effects.

The present results might be used in future studies for modeling the stochastic cohesive behavior of the concrete at a mesoscopic scale considering a precise description of the aggregate shapes and localizations in mesoscopic concrete samples (see Lhonneur 2021). In particular, such statistical numerical studies might serve to identify Representative Elementary Volumes (REV) for fracture processes in concrete samples.

Acknowledgements

Authors are grateful to the LMGC technical team as well as to F. Gbekou for their useful support in experimental matters.

References

Simonova, H., Vyhlidal, B., Kurcharczykova, B., Bayer, P., Kersner, Z., 2017. Modelling of interfacial transition zone effect on resistance to crack propagation in fine-grained cement-based composites. Frattura ed Integrità Strutturale 41, 211-219.

Samal, D.K., Ray, S., Hemalatha, T., 2019. Effect of interfacial transition zone on fracture energy in concrete, 10th International Conference on Fracture Mechanics of Concrete and Concrete Structures FraMCoS-X.

Gu, X., Hong, L., Wang, Z., Lin, F., 2013. Experimental study and application of mechanical properties for the interface between cobblestone aggregate and mortar in concrete. Construction and Building Materials 46, 156-166.

Mielniczuk, B., Jebli, M., Jamin, F., El Youssoufi, M.S., Pelissou, C., Monerie, Y., 2015. Characterization of behavior and cracking of a cement paste confined between spherical aggregate particles. Cement and Concrete Research 79, 235-242.

Jebli, M., Jamin, F., Malachanne, E., Garcia-Diaz, E., El Youssoufi, M.S., 2018. Experimental characterization of mechanical properties of the cement-paste aggregate interface in concrete. Construction and Building Materials 161, 16-25.

Malachanne, E., Jebli, M., Jamin, F., Garcia-Diaz, E., El Youssoufi, M.S., 2018. A cohesive zone model for the characterization of adhesion between cement paste and aggregates. Construction and Building Materials 193, 64-71.

Salah, N., Jebli, M., Malachanne, E., Jamin, F., Dubois, F., Caro, A.S., Garcia-Diaz, E., El Youssoufi, M.S., 2019. Identification of a cohesive zone model for cement paste-aggregate interface in a shear test. European Journal of Environmental and Civil Engineering, 1-15.

Martin, E., Vandellos, T., Leguillon, D., Carrère, N., 2016. Initiation of edge debonding: coupled criterion versus cohesive zone model. International Journal of Fracture 199, 157-168.

Leguillon, D., 2002. Strength or Toughness? A criterion for crack onset at a notch. European Journal of Mechanics A/Solids 21, 61-72.
Lhonneur, J., 2021. Approche par changement d'échelle du vieillissement des bétons : expérimentations et simulations numériques. PhD thesis, University of Montpellier.